Orthotropic Thin Shell Elasticity Estimation for Surface Registration

Qingyu Zhao[1], Stephen Pizer[1,2], Ron Alterovitz[1], Marc Niethammer[1], and Julian Rosenman[2,1]

[1] Computer Science, UNC Chapel Hill, NC, United States
[2] Radiation Oncology, UNC Chapel Hill, NC, United States

Abstract. Elastic physical models have been widely used to regularize deformations in different medical object registration tasks. Traditional approaches usually assume uniform isotropic tissue elasticity (a constant regularization weight) across the whole domain, which contradicts human tissue elasticity being not only inhomogeneous but also anisotropic. We focus on producing more physically realistic deformations for the task of surface registration. We model the surface as an orthotropic elastic thin shell, and we propose a novel statistical framework to estimate inhomogeneous and anisotropic shell elasticity parameters only from a group of known surface deformations. With this framework we show that a joint estimation of within-patient surface deformations and the shell elasticity parameters can improve groupwise registration accuracy. The method is tested in the context of endoscopic reconstruction-surface registration.

1 Introduction

A popular way of solving medical image registration problems is to formulate an optimization that minimizes a weighted sum of two energy terms: data mismatch and the *regularity* of the deformation that deforms one data item to the other. In particular, the latter term has been formulated from different standpoints, one of which is to use physical energy derived from an *elastic model* to regularize deformations [1]. Even though some other methods [2,3,4] have also produced reasonable results via different regularization formulations, the elasticity-model-based idea is particularly appealing because in many medical applications anatomical deformations are indeed elastic processes caused by muscles or other forces.

The key to realistic physical modeling is to apply proper elasticity parameters. As a matter of fact, human tissue elasticity is both *inhomogeneous* (different tissue types show different stiffness) [5] and *anisotropic* (e.g., different stiffness along and across the tissue fiber direction) [6]. However, traditional registration approaches simply assume a spatially constant elasticity parameter (the single regularization weight), which makes the physical modeling unrealistic. Therefore, the use of elasticity models in registration currently becomes more of a motivational concept than the seeking of truly physical deformations. The above

argument motivates research interest in studying spatially varying tissue elasticity, not only for registration, but also for simulation [7] and pathology analysis [8]. However, most approaches for non-uniform elasticity estimation have to use a sophisticated mechanical system equipped with a force generation/measurement capability, which is often unavailable in a common registration setting.

In this paper, we propose a statistical framework that can estimate spatially varying anisotropic elasticity parameters only using a set of known material deformations. In particular, we focus on studying a physical model for registration of anatomic surfaces that have deformed within a patient. We first propose to model the surface as an orthotropic elastic thin shell. To be specific, *orthotropy* is a special kind of anisotropy that can characterize different material stiffness along different directions, but the orthotropic model has fewer parameters than arbitrary anisotropy. Next we show that with some proper prior knowledge, spatially inhomogeneous and orthotropic elasticity parameters can be estimated from a set of known shell (surface) deformations via a novel *maximum-a-posteriori* (MAP) optimization. We finally show that with this statistical framework we can improve the groupwise surface registration accuracy by a joint estimation of surface deformations and shell elasticity parameters.

We test this framework in the context of endoscopy 3D reconstruction, the goal of which is to produce a 3D reconstruction surface from multiple endoscopic movie frames. Since the tissue is constantly deforming during endoscopy, a key step of this reconstruction is to register all the single-frame 3D reconstruction surfaces into a unified surface to account for the aforementioned deformations across frames. We show that our elasticity estimation framework is able to retrieve insightful tissue elastic properties from the data and in turn to improve this groupwise registration.

1.1 Related Work

Closely related to our work is a research branch known as *spatially-varying registration*, the idea of which is to let regularization strength be dependent on location. This can be modeled by spatially-varying diffusion [9], non-stationary Gaussian processes [10] or applying a non-stationary metric in the LDDMM setting [11]. Despite their theoretical appeal, those methods explore the problem mostly from the computational aspect and lack physical motivation, and they also don't handle the anisotropic situation. The notion of spatially-varying registration has been also used in elastic models [12,13], but the elasticity parameters have to be manually chosen for known segmented regions.

Automatic elasticity estimation has been studied in different medical applications [14,6]. With tissue displacements and external forces taken as known values, the elasticity can be computed directly as an inverse problem of the Finite Element Method (FEM). Elastography is another widely used non-invasive procedure for determining local elastic properties, but it either requires a force exertion/measurement device or a vibration actuation mechanism [15], which is often not available in other imaging modalities.

Therefore, *modality-independent* and purely *image-based* approaches are desired and have been under investigation for several years. Miga et. al. [5] introduced registration-based elastography to estimate tissue stiffness of an object given two images of it undergoing an elastic deformation. Risholm et. al. [16] extended this approach by forming a probabilistic model over the registration parameters and inhomogeneous isotropic elasticity parameters. While our framework is related to theirs, ours is different by incorporating anisotropy and by applying the model to surface data.

In a broader context, *Statistical Shape Analysis* seeks a statistical distribution or a low dimensional subspace, called a shape space, for describing a given set of shapes (or shape deformations). Most existing approaches [17,18] construct the shape space by constraining the shape's global appearance, such as deformation vector fields, point positions or normal directions. Our framework provides an alternative perspective in the sense that it recovers the underlying physical reason that can best explain the given shape deformations.

2 Orthotropic Thin Shell

Thin shells are special 3D structures bounded by two curved surfaces (Fig. 1a), where the distance between the surfaces (thickness) is small in comparison with other body dimensions (width). Due to this high width-to-thickness ratio, the behavior of a thin shell can be characterized by its middle surface $\mathcal{M}$, the locus of points that lie at equal distances from the two bounding surfaces. In this situation, out-of-plane strain can be neglected, and the elastic model is reduced to 2D. The 2D linear *Hooke's law* for arbitrary anisotropy reads

$$\sigma = [\sigma_{xx}, \sigma_{yy}, \sigma_{xy}]^T = C[\varepsilon_{xx}, \varepsilon_{yy}, \varepsilon_{xy}]^T = C\varepsilon, \tag{1}$$

where σ and ε are the *local* in-plane stress and strain tensors parameterized on the tangent plane of the middle surface $\mathcal{M}$, and C is a 3×3 positive definite matrix, called a *stiffness matrix*, characterizing *local* elasticity .

For a thin shell, it can be shown that the *local* strain ε can be classified into the stretching strain φ and bending strain κ, where the relationship between ε and $\{\varphi, \kappa\}$ follows the *Love-Kirchhoff hypothesis* [19,20]. The *local* deformation energy is approximated by the function W:

$$W(\varphi, \kappa, C) = \lambda_s \varphi^T C \varphi + \lambda_b \kappa^T C \kappa, \tag{2}$$

where $\varphi = [\varphi_{xx}, \varphi_{yy}, \varphi_{xy}]^T$ is the tangential Cauchy-Green strain tensor characterizing local stretching, $\kappa = [\kappa_{xx}, \kappa_{yy}, \kappa_{xy}]^T$ is the shape operator difference characterizing local bending (local curvature change), and $\{\lambda_s, \lambda_b\}$ are the global mixing weights determined by shell thickness.

Orthotropic material is a special type of anisotropic material. For an orthotropic shell, the anisotropy on the tangent plane is symmetric w.r.t. two orthogonal axes, known as the *natural axes*. This leads to a simplified stiffness

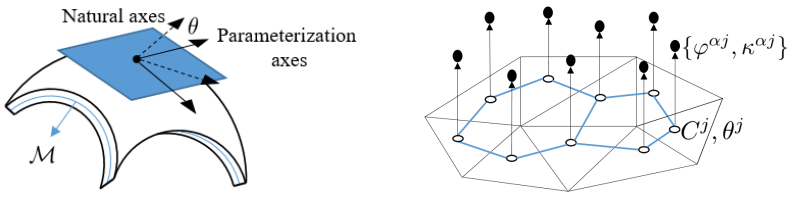

(a) (b)

Fig. 1: (a) A thin shell model. (b) A Gaussian MRF model with nodes (white) defined on the dual graph (blue) of a triangle mesh. Node j (triangle $\mathcal{T}^j$) is associated with unknown variables (C^j, θ^j) and a set of observed variables $\{\varphi^{\alpha j}, \kappa^{\alpha j} | \alpha = 1...N\}$

matrix in the following form when σ and ε are parameterized under this natural-axes coordinate system:

$$C = \begin{bmatrix} c_1 & c_2 & 0 \\ c_2 & c_3 & 0 \\ 0 & 0 & c_4 \end{bmatrix} = \frac{1}{1 - \nu_{xy}\nu_{yx}} \begin{bmatrix} E_x & \nu_{vu}E_x & 0 \\ \nu_{xy}E_y & E_y & 0 \\ 0 & 0 & 2G_{xy}(1 - \nu_{xy}\nu_{yx}) \end{bmatrix}, \quad (3)$$

where $\{E_x, E_y\}$ are the Young's moduli along the natural axes, $\{\nu_{xy}, \nu_{yx}\}$ are the Poisson's ratios, and G_{xy} is the shear modulus. In the following text, we will use C to denote such a simplified matrix, called the *canonical orthotropic stiffness matrix*. We denote the space of such matrices as $\mathbf{SPD}_C$.

Rotation of Frame. When σ and ε are parameterized under an arbitrary orthogonal frame (Fig. 1a) instead of rotated into the natural axes, we have the following relationship,

$$\begin{bmatrix} \varepsilon_{xx} & \varepsilon_{xy} \\ \varepsilon_{xy} & \varepsilon_{yy} \end{bmatrix} = \begin{bmatrix} cos(\theta) & sin(\theta) \\ -sin(\theta) & cos(\theta) \end{bmatrix} \begin{bmatrix} \varepsilon'_{xx} & \varepsilon'_{xy} \\ \varepsilon'_{xy} & \varepsilon'_{yy} \end{bmatrix} \begin{bmatrix} cos(\theta) & -sin(\theta) \\ sin(\theta) & cos(\theta) \end{bmatrix}, \quad (4)$$

where $\{\varepsilon'_{\alpha\beta}\}$ is the strain tensor parameterized under an arbitrary orthogonal frame and θ is the rotation angle between the two frames, known as the *canonical angle*. The same rotational relationship applies for σ. Combining with Eq. 1, the stiffness matrix under an arbitrary frame is $C' = R^{-1}CR$, where

$$R = \begin{bmatrix} cos(\theta)^2 & sin(\theta)^2 & 2cos(\theta)sin(\theta) \\ sin(\theta)^2 & cos(\theta)^2 & -2cos(\theta)sin(\theta) \\ -cos(\theta)sin(\theta) & cos(\theta)sin(\theta) & cos(\theta)^2 - sin(\theta)^2 \end{bmatrix}. \quad (5)$$

In other words, C and θ uniquely determines the *local* orthotropic stiffness matrix parameterized under an arbitrary frame.

The orthotropic elasticity model has shown its effectiveness in modeling 3D soft tissues in the situations where the stiffness is usually different in a direction parallel to the fibers than in the transverse directions [6,7]. We adapt this model to the essentially 2D situation of the physical thin shell model Zhao et. al [21] proposed for surface registration.

3 Elasticity Estimation via MAP

We assume some observed material deformations are the realization of tissue elasticity of a single patient. Then a common way to estimate elasticity parameters is to solve an inverse problem given such deformations and external force measurements. However, when only the material deformations are available, the parameter estimation can be highly ill-posed. Therefore, we opt for energy-based models that are commonly used in statistical mechanics. In these models high probability states are associated with low energy configurations. Here we propose a *Physical-Energy-Based Markov Random Field* (MRF) model to estimate the elasticity parameters from a probabilistic point of view.

Problem Statement. With some abuse of notation we use $\mathcal{M}$ to represent both a shell and its middle surface domain. Given a reference shell $\mathcal{M}$ and a set of N example deformations $\boldsymbol{\mathcal{D}} = \{\mathcal{D}^\alpha : \mathcal{M} \to \mathbb{R}^3 | \alpha = 1...N\}$, our goal is to find the canonical orthotropic stiffness matrix function $\mathbf{C} : \mathcal{M} \to \mathbf{SPD}_C$ and the canonical angle function $\boldsymbol{\theta} : \mathcal{M} \to \mathbf{S}^1$, namely the orthotropic elasticity parameters of every location on the shell. To simplify the problem, we start off by discretizing the continuous shell $\mathcal{M}$ to a triangle-mesh $\{\mathcal{T}^j | j = 1...M\}$ with M triangles. We associate each triangle $\mathcal{T}^j$ with its own local elasticity parameters (C^j, θ^j). Each deformation $\mathcal{D}^\alpha$ is then reparameterized locally on the tangent planes (triangles). In other words, each triangle $\mathcal{T}^j$ has its own local stretching strain $\varphi^{\alpha j}$ and bending strain $\kappa^{\alpha j}$. Finally, the goal is to estimate the set of elasticity parameters $(\mathbf{C}, \boldsymbol{\theta}) = \{C^j, \theta^j\}$ given the set of local strains $\{\varphi^{\alpha j}, \kappa^{\alpha j}\}$.

The MRF Model. Our idea is that the elasticity parameters that "best fit" the observed deformations should yield small total elastic deformation energy. Meanwhile, we assume the parameters should vary smoothly across the shell. Finally, due to the scale ambiguity caused by the lack of external force measurements [8,16], we assign the parameters with a prior to avoid the trivial solution (similar to [8,16], we compute parameters relative to the prior).

We build an MRF model on the dual graph of the triangle mesh as shown in Fig. 1b. Each node on the graph represents the elasticity parameters associated with the underlying triangle. We want to find $(\mathbf{C}, \boldsymbol{\theta})$ to maximize the posterior distribution $p(\mathbf{C}, \boldsymbol{\theta} | \boldsymbol{\mathcal{D}})$:

$$p(\mathbf{C}, \boldsymbol{\theta} | \boldsymbol{\mathcal{D}}) \propto p(\boldsymbol{\mathcal{D}} | \mathbf{C}, \boldsymbol{\theta}) p(\mathbf{C}, \boldsymbol{\theta}). \tag{6}$$

The likelihood $p(\boldsymbol{\mathcal{D}} | \mathbf{C}, \boldsymbol{\theta})$ is associated with the total deformation energy of all example deformations. Assuming local deformation energy follows independent Boltzmann distributions, we design our the likelihood as the following:

$$p(\boldsymbol{\mathcal{D}} | \mathbf{C}, \boldsymbol{\theta}) = \prod_\alpha \prod_j p(\varphi^{\alpha j}, \kappa^{\alpha j} | C^j, \theta^j) \propto \prod_\alpha \prod_j \exp(-W(\varphi^{\alpha j}, \kappa^{\alpha j}, C^j, \theta^j)) \tag{7}$$

Consider the prior distribution of $(\mathbf{C}, \boldsymbol{\theta}) = \{C^j, \theta^j\}$, the second term of Eq. 6. Following the idea from Gaussian MRFs, each node has its own per-node prior function ψ_j, and each edge has an edge potential function ψ_{jk}:

$$p(\mathbf{C}, \boldsymbol{\theta}) \propto \prod_j \psi_j(C^j) \prod_{j,k} \psi_{jk}(C^j, \theta^j, C^k, \theta^k). \tag{8}$$

The ψ_{jk} function models the spatial smoothness nature of the shell's orthotropic property by penalizing the difference of stiffness matrices between neighbouring nodes and the smoothness of the natural-axes direction field. We assume $\boldsymbol{C}$ and θ are independent and design

$$\psi_{jk}(C^j, \theta^j, C^k, \theta^k) \propto \exp(-d(C^j, C^k)^2) \cdot \exp(-(p_{jk}(\theta^j) - \theta^k)^2), \tag{9}$$

where $d(\cdot, \cdot)$ is a proper distance metric for $\mathbf{SPD}_C$. We use the Log-Euclidean metric [22] for its computational convenience. $p(\cdot)$ is the Levi-Civita parallel transport operation [23] that transports a vector associated with θ_j from $\mathcal{T}^j$ to the neighbouring triangle $\mathcal{T}^k$.

For the per-node prior function ψ_j, we assume anisotropy is distributed in a Gaussian sense with the isotropic case being the mean situation. Therefore, given an isotropic prior Young's modulus E and Poisson's ratio ν, we design $\psi_j(C^j) \propto exp(-d(C^j, \bar{C})^2)$, where $\bar{C}$ is the commonly used isotropic stiffness matrix derived from E and ν. Finally, we optimize the negative log posterior in the following form:

$$\begin{aligned} -\log\, p(\mathbf{C}, \boldsymbol{\theta}|\boldsymbol{\mathcal{D}}) = &\sum_{j,k} [\lambda_1 d(C^j, C^k)^2 + \lambda_2 (p_{jk}(\theta^j) - \theta^k)^2] + \\ &\sum_{\alpha} \sum_{j} W(\epsilon^{\alpha j}, \kappa^{\alpha j}, C^j, \theta^j) + \sum_{j} \lambda_3 d(C^j, \bar{C})^2 \end{aligned} \tag{10}$$

where the λ parameters are the global weights.

4 Joint Estimation of Registration and Elasticity

In many groupwise registration analysis [24], both the material deformations and elasticity parameters are unknown variables. Formally, we want to investigate the joint probability of the group of deformations $\boldsymbol{\mathcal{D}}$ and elasticity parameters $(\mathbf{C}, \boldsymbol{\theta})$, given a reference shell $\mathcal{M}$ and its many deformed version $\{\mathcal{M}^\alpha | i = \alpha ... N\}$. A common approach is to treat one set of variables, e.g., $(\mathbf{C}, \boldsymbol{\theta})$, as latent variables and perform an *Expectation-Maximization* algorithm to estimate the posterior

$$p(\boldsymbol{\mathcal{D}}|\mathcal{M}, \{\mathcal{M}^i | i = 1...N\}) = \int_{\mathbf{C}, \boldsymbol{\theta}} p(\boldsymbol{\mathcal{D}}, \mathbf{C}, \boldsymbol{\theta}|\mathcal{M}, \{\mathcal{M}^i | i = 1...N\}). \tag{11}$$

In this study, we opt for a simple *alternating optimization* algorithm that uses the mode over the $(\mathbf{C}, \boldsymbol{\theta})$ parameters to approximate the posterior for computational simplicity.

Our alternating optimization approach iterates between the following steps:

1. *Input*: a reference shell $\mathcal{M}$ and a set of deformed shells $\{\mathcal{M}^\alpha | \alpha = 1...N\}$. The elasticity parameters are initialized to be $\bar{C}$ everywhere.

2. With the current estimate of $(\mathbf{C}, \boldsymbol{\theta})$, perform MAP on

$$p(\boldsymbol{\mathcal{D}}|\mathbf{C}, \boldsymbol{\theta}, \mathcal{M}, \{\mathcal{M}^\alpha|\alpha = 1...N\}) = \prod_{\alpha=1}^{N} p(\mathcal{D}^\alpha|\mathbf{C}, \boldsymbol{\theta}, \mathcal{M}, \mathcal{M}^\alpha) \qquad (12)$$

This step is essentially a set of independent pairwise surface registrations between $(\mathcal{M}, \mathcal{M}^\alpha)$ with inhomogeneous and orthotropic energy as the deformation regularization. We adopt the Thin Shell Demons method [21] to accomplish this step. It uses curvature-based geometric features to drive the deformation and allows thin-shell-based elastic regularization.

3. Using the framework in Section 3, perform MAP on $p(\mathbf{C}, \boldsymbol{\theta}|\mathcal{D}, \mathcal{M})$ with the deformations estimated from Step 2 to update the elasticity parameter.

4. Iterate to Step 2 until convergence.

5 Experiments

Proof of Concept. In this experiment we tested on a toy example the capability of elasticity parameter estimation from known deformations without any registration involved. We mainly investigated the estimation accuracy of the canonical angle and the two Young's moduli, which are the three most important parameters in characterizing local orthotropy. A bar-shaped surface shown in Fig. 2a was manually assigned ground truth elasticity parameters (Fig. 2b), including both the orthotropic canonical stiffness matrices and natural axes directions. The bar is more elastic at the center (inhomogeneity) and more elastic along the vertical direction (orthotropy). The other elasticity parameters were set to satisfy $\nu_{xy}\nu_{yx} = 0.25^2$ and $G_{xy} = 2kPa$. We created 20 synthetic deformations to the bar (Fig. 2c) by first fixing its two ends at random positions as boundary constraints and then optimizing Eq. 7 to solve for the deformations using ground truth elasticity. We tested our framework introduced in Section 3 to estimate the elasticity parameters from this set of simulated deformations. The weighting parameters $\{\lambda_1 = 1, \lambda_2 = 10, \lambda_3 = 0.1\}$ were chosen empirically to best fit this toy problem. We found that the natural axes first have to be accurate to yield meaningful anisotropy, so we set a larger λ_2 to regularize the vector field. Other model parameters $\{\lambda_s = 80, \lambda_b = 10\}$ and the isotropic prior $\{E = 2\text{kPa}, \nu = 0.25\}$ were chosen the same as in [24]. Fig. 2d shows the two estimated Young's moduli and the estimated natural axes directions. The average canonical angle error is 0.74 degree, which shows we can successfully estimate the natural axes directions. Fig 2e shows that with the estimated orthotropic elasticity parameters the simulated deformation is more accurate in the sense that the center-elastic part has a larger bending effect than the one simulated from isotropic elasticity under the same boundary constraints.

Synthetic Head-and-Neck Data. We tested joint registration and elasticity parameter estimation with synthetic deformations on 5 real patients' head-and-neck CT data. In particular, a pharyngeal surface (Fig. 3a) from the pharynx

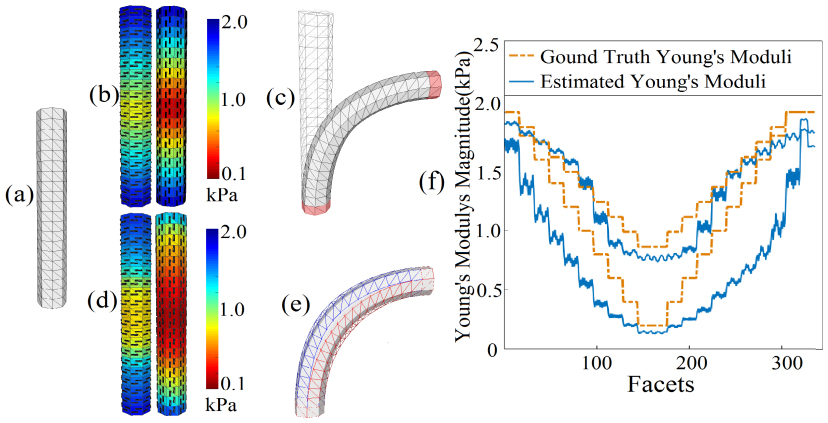

Fig. 2: (a) A reference bar-shaped surface. (b) The two ground truth Young's moduli are respectively color-coded across the surface. Red regions indicate smaller Young's moduli (more elastic). Each local Young's modulus is associated with a natural axis direction (black vector fields) (c) A deformed surface derived from ground truth elasticity. Red regions are the fixed boundary constraints. (d) Estimated Young's moduli and the associated estimates of natural axes. (e) Deformed surfaces derived from ground truth elasticity (blue wireframe), estimated elasticity (gray surface) and isotropic elasticity (red frame). (f) The two ground truth Young's moduli (the orange curves) and the two estimated Young's moduli (the blue curves) on all faces.

down to the vocal cord was segmented from a 3D CT image. Each surface has about 6k facets. We manually assigned ground truth orthotropic elasticity parameters and natural axes directions to the reference surface to reflect known anatomical facts: the epiglottis being stiffer than the vallecula and the pharyngeal wall being more elastic cross-sectionally (Fig. 3b). Similar to the previous example, we simulated 20 synthetic deformations to each patient's surface by assigning 20 manually constructed boundary conditions. These deformations include the expansion/compression of the pharyngeal wall and the opening/closing of the larynx. These deformations were also used as ground truth deformations for testing the accuracy of the later registration. We tuned down λ_1 to 0.1 to avoid overly smoothing the estimation. All the other algorithm parameters were kept the same.

To further test the elasticity estimation framework, we first estimated the elasticity parameters directly from the ground truth deformations (not for the registration purpose). Fig. 3c shows that the general pattern of the two Young's moduli and the natural axes can be reasonably recovered, but the scale difference with the ground truth suggests our method only recovers parameters up to a scale relative to the prior isotropic elasticity. Moreover, the elasticity-smoothness term in Eq.10 tends to yield blurred estimation. Due to these artifacts, the

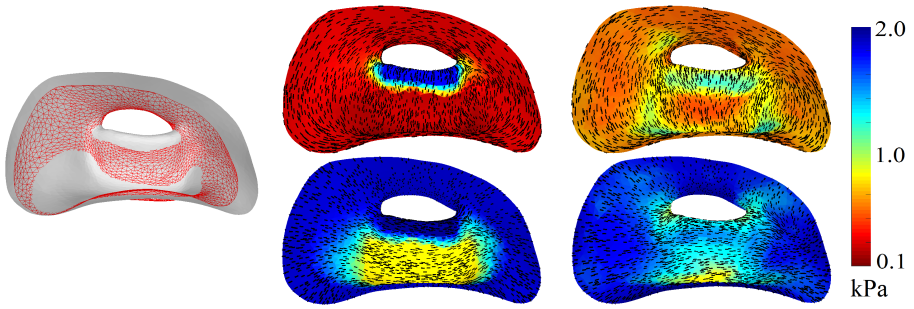

(a) (b) (c)

Fig. 3: (a) A pharyngeal CT segmentation surface (gray surface) and one of its synthetic deformations (red wireframe). (b) Ground truth Young's Moduli along the two natural axes. The epiglottis (blue region in the top figure) is set to be stiffer than the vallecula (yellow region in the bottom figure). (c) Estimated elasticity using ground truth deformations.

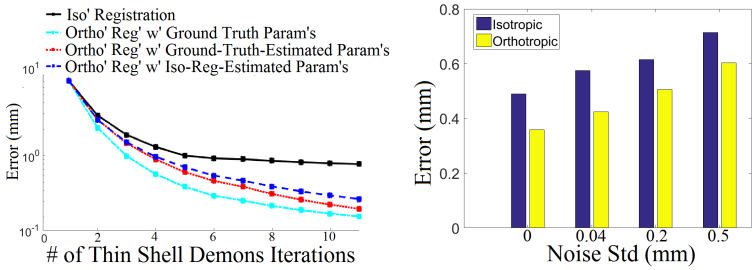

(a) (b)

Fig. 4: (a) Registration accuracy over registration iterations under different options. (b) Final registration accuracy under different levels of noise.

average error over all facets for the two Young's moduli are 0.41kPa and 0.38kPa respectively. The average canonical angle error is 12 degrees.

To test joint estimation accuracy, we performed one iteration of the framework introduced in Section 4. To be specific, we first performed 20 independent registrations between the reference surface and the 20 deformed surfaces using isotropic elasticity, followed by an elasticity estimation using the 20 resulting deformations. This gives us estimated orthotropic elasticity across the reference surface for a second round of registrations. Fig. 4a gives accuracy measurement under different registration options. The error is computed as the average per-vertex Euclidean distance error (compared against the aforementioned ground truth deformations) over all vertices and all 3 patients. Note that the x-axis in Fig. 4a denotes the iterations within the Thin Shell Demons [21] registration,

not to be confused with the overall joint estimation iteration discussed in Section 4. The 2^{nd}-round orthotropic registration (blue curve) performs better than the isotropic registration (black). Meanwhile, it is only slightly worse than using orthotropic elasticity estimated directly from ground truth deformations. This means that further elasticity update won't improve the results too much.

We also tested the robustness of this joint estimation framework under the effect of noise. Different levels of white Gaussian noise were added to all vertices. Fig. 4b shows that the 2^{nd}-round orthotropic registration performs better than the isotropic registration in all 4 cases.

Real Endoscopic Data. We further used our framework to investigate the pharyngeal deformations contained in live nasopharyngoscopy. An endoscopic video provides direct visualization of a patient's pharyngeal surface and usually captures its rich swallowing motion. Elasticity estimation on this frame-by-frame surface deformation can help us better understand tissue characteristics and facilitate further analysis, such as the registration between the endoscopy and CT of the same patient for radiation treatment planning.

We first reconstructed a surface model from the video as the reference surface $\mathcal{M}$. This reconstructed surface, called an endoscopogram, was computed by first applying Shape-from-Motion-and-Shading (SfMS) [25] to produce a set of N single-frame reconstructions $\{\mathcal{M}^\alpha | \alpha = 1...N\}$ and then fusing $\{\mathcal{M}^\alpha | \alpha = 1...N\}$ into a unified and complete surface $\mathcal{M}$ [24]. Next, we computed the set of deformations $\boldsymbol{\mathcal{D}} = \{\mathcal{D}^\alpha | \alpha = 1...N\}$ from the endoscopogram $\mathcal{M}$ to each single-frame reconstruction by using independent isotropic registration. Finally, we applied our elasticity estimation framework on $\boldsymbol{\mathcal{D}}$ and $\mathcal{M}$. The algorithm parameters used in this experiment were the same as before.

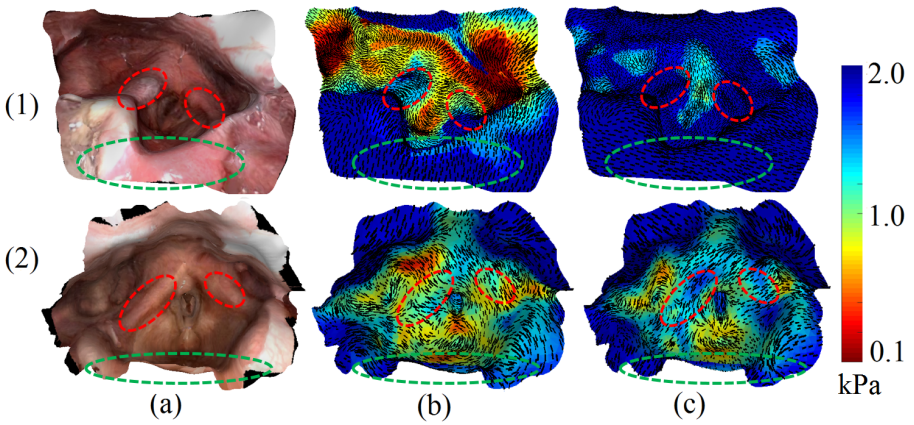

Fig. 5: (a) Endoscopogram surfaces reconstructed from video. Red circles indicate the arytenoid cartilage. Green circles indicate the epiglottis. (b)(c) Estimated Young's moduli and the associated natural axes.

We tested on two patients' endoscopic video data. For each video sequence we sampled 20 individual frames focusing on the laryngeal region to produce the endoscopogram. Fig. 5 shows the results are consistent with throat anatomy: the epiglottis and the arytenoid cartilage be stiffer than the laryngeal region, the larynx being more elastic along the patient axial direction.

6 Discussion

We have introduced a statistical framework to estimate inhomogeneous and anisotropic elasticity parameters of a thin shell structure from a set of its known deformations. We have shown that an MAP analysis on a novel MRF-based probability distribution can automatically recover both the orthotropic stiffness matrix and natural axes directions of every location on the shell. We have also shown that this framework can be further used as a part in a joint registration and elasticity estimation framework. Both the elasticity estimation framework and the joint estimation framework can be helpful in studying within-patient deformations of anatomical surfaces. Despite the promising results shown in our experiments, we still have to address the following concerns in future work:

1. In many situations anatomical surfaces are deformed by the underlying muscles, so it is not appropriate to simply model the surface as a shell structure. We should generalize our framework to the 3D volume situation.

2. Model parameters selection needs to be further studied.

3. In several real endoscopic cases, real tissue deformations were dominated by other non-physical deformations (e.g. reconstruction errors). The applicability of our framework in this situation needs to be further examined.

Acknowledgement This work was supported by NIH grant R01 CA158925. We thank Dr. Bhisham Chera from the Department of Radiation Oncology for providing the endoscopy data.

References

1. Bajcsy, R., Kovačič, S.: Multiresolution elastic matching. Computer Vision, Graphics, and Image Processing **46**(1) (1989) 1–21
2. Christensen, G., Rabbitt, R., Miller, M.: Deformable templates using large deformation kinematics. Computer Vision, Graphics, and Image Processing **5**(10) (1996) 1435–1447
3. Thirion, J.: Image matching as a diffusion process: an analogy with Maxwells demons. Medical Image Analysis **2**(3) (1998) 243–260
4. Beg, M., Miller, M., Trouvé, A., Younes, L.: Computing large deformation metric mappings via geodesic flows of diffeomorphisms. International Journal of Computer Vision **61**(2) (2005) 139–157
5. Miga, M.: A new approach to elastography using mutual information and finite elements. Physics in Medicine and Biology **48**(4) (2003)
6. Kroon, M., Holzapfel, G.A.: Estimation of the distributions of anisotropic, elastic properties and wall stresses of saccular cerebral aneurysms by inverse analysis. Proceedings of the Royal Society of London A: Mathematical, Physical and Engineering Sciences **464**(2092) (2008) 807–825

7. Schneider, R., Faust, G., Hindenlang, U., Helwig, P.: Inhomogeneous, orthotropic material model for the cortical structure of long bones modeled on the basis of clinical CT or density data. Computer Methods in Applied Mechanics and Engineering **198**(27-29) (2009) 2167–2174
8. Yang, S., Jojic, V., Lian, J., Chen, R., Zhu, H., Lin, M.C.: Classification of prostate cancer grades and t-stages based on tissue elasticity using medical image analysis. In: MICCAI. (2016) 627–635
9. Freiman, M., Voss, S.D., Warfield, S.K.: Demons registration with local affine adaptive regularization: application to registration of abdominal structures. In: IEEE International Symposium on Biomedical Imaging. (2011) 1219C1222
10. Gerig, T., Shahim, K., Reyes, M., Vetter, T., Lüthi, M.: Spatially varying registration using gaussian processes. In: MICCAI. (2014) 627–635
11. Vialard, F.X., Risser, L.: Spatially-varying metric learning for diffeomorphic image registration: A variational framework. In: MICCAI. (2014) 227–234
12. Davatzikos, C.: Spatial transformation and registration of brain images using elastically deformable models. Computer Methods in Applied Mechanics and Engineering **66**(2) (1997) 207–222
13. Alterovitz, R., Goldberg, K., Pouliot, J., Hsu, I.C.J., Kim, Y., Noworolski, S.M., Kurhanewicz, J.: Registration of MR prostate images with biomechanical modeling and nonlinear parameter estimation. Med. Phys. **33**(2) (2006) 446–454
14. Misra, S., Ramesh, R., Okamura, A.: Modelling of non-linear elastic tissues for surgical simulation. Computer Methods in Applied Mechanics and Engineering **13**(6) (2010) 811–818
15. Green, M., Geng, G., Qin, E., Sinkus, R., Gandevia, S., Bilston, L.: Measuring anisotropic muscle stiffness properties using elastography. NMR Biomed **26**(11) (2013) 1387–1394
16. Risholm, P., Ross, J., Washko, G., Wells, W.: Probabilistic elastography: estimating lung elasticity. In: IPMI. (2011) 699–710
17. Bauer, M., Bruveris, M., Michor, P.W.: Overview of the geometries of shape spaces and diffeomorphism groups. J Math Imaging Vis **50**(1) (2014) 60–97
18. Schulz, J., Pizer, S.M., Marron, J., Godtliebsen, F.: Nonlinear hypothesis testing of geometrical object properties of shapes applied to hippocampi. Journal of Mathematical Imaging and Vision **54**(1) (2015) 15–34
19. Ventsel, E., Krauthammer, T.: Thin Plates and Shells: Theory: Analysis, and Applications. CRC Press (2001)
20. Gingold, Y., Secord, A., Han, J.Y., Grinspun, E., Zorin, D.: A discrete model for inelastic deformation of thin shells. Technical report, Courant Institute of Mathematical Sciences (2004)
21. Zhao, Q., Price, J.T., Pizer, S., Niethammer, M., Alterovitz, R., Rosenman, J.: Surface registration in the presence of topology changes and missing patches. In: Medical Image Understanding and Analysis. (2015) 8–13
22. Arsigny, V., Fillard, P., Pennec, X., Ayache, N.: Log-euclidean metrics for fast and simple calculus on diffusion tensors. Phys Med Biol **56**(2) (2006) 411–421
23. Crane, K., Desbrun, M., Schröder, P.: Trivial connections on discrete surfaces. In: Symp. on Geometry Proc. Volume 29. (2010)
24. Zhao, Q., Price, T., Pizer, S., Niethammer, M., Alterovitz, R., Rosenman, J.: The endoscopogram: A 3D model reconstructed from endoscopic video frames. In: MICCAI. (2016) 439–447
25. Price, T., Zhao, Q., Rosenman, J., Pizer, S., Frahm, J.M.: Shape from motion and shading in uncontrolled environments. Technical report, Department of Computer Science, University of North Carolina at Chapel Hill (2016)